CELL MEMBRANE FEATURE DETECTION USING GRAPH NEURAL NETWORKS

Edward Offord, E. Josiah Lutton, Till Bretschneider

Department of Computer Science, University of Warwick, Coventry CV4 7AL, United Kingdom

ABSTRACT

Many cellular processes involve complex deformations of the cell surface, which are difficult to automatically detect and analyse in 3D microscopy images. One issue faced by modern machine learning methods is that 3D microscopy images are large and require a high computational load to analyse. To simplify this problem, we propose a graph convolutional neural network applied to a triangulated mesh of the cell surface, where nodes are associated with geometric and intensity features of biomarkers on or near the surface. Here, we focus on identification of macropinocytic cups on the surface of *Dictyostelium* cells, structures involved in the uptake of extracellular fluid. The network classifies each node into belonging to a cup or not, enabling subsequent studies of the detailed distribution of molecules regulating fluid uptake in cells. We show that a simple network architecture can identify key features of the surface, suggesting that these methods have strong potential for advancing the analysis of cell surface dynamics.

***Index Terms*—** Macropinocytosis, Microscopy, Cell Biology, Graph Convolutional Neural Networks

1. INTRODUCTION AND RELATED WORK

The cytoplasmic membrane is fundamental in integrating cell signalling and cellular mechanics. Recent advances in microscopy and whole-cell segmentation methods (for example [1, 2, 3]) make it possible to capture highly complex dynamic cell surfaces in 3D, at an unprecedented level of detail. However, analysis of the detailed structure of these surfaces presents a major challenge. One option is to classify features directly in 3D images [4, 5, 6], but restricting the problem to analysing the cell surface as a triangulated mesh can dramatically reduce the computational load. A linear SVM has been shown to accurately classify simple motifs on cell surfaces, but the surface needs to be split into convex patches first [7].

We propose the use of graph convolutional neural networks (GCNs) as the ideal tool for feature detection on the closed surface mesh. GCNs are analogous to convolutional neural networks used in image processing, but are able to account for the irregular structure of a graph [8]. Graph neural networks have previously been applied to other biomedical imaging problems (e.g. [9, 10]), and more broadly in bioinformatics [11].

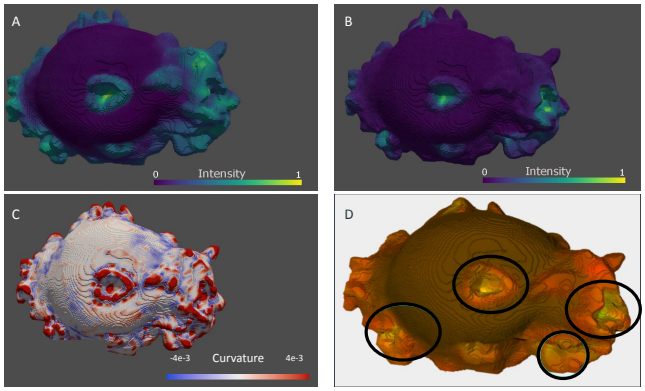

Fig. 1. Triangulated surface of a *Dictyostelium* cell with macropinocytic cups, expressing fluorescent markers for PIP3 and actin. PIP3 is a signalling molecule localizing cups. Actin is a cytoskeletal protein, providing the mechanical force to shape cups. Vertex colours represent intensities for **A**: Actin; **B**: PIP3; **C**: Areas of positive (red) and negative (blue) Gaussian curvature; **D**: Actin (red) and PIP3 (green) channels merged, cups encircled in black.

Here we use GCNs for segmenting crown-like structures known as cups on the surface of a *Dictyostelium* cell, as shown in Figure 1, which are involved in non-specific extracellular fluid uptake (macropinocytosis [12]). Macropinocytosis is used by cancer cells for feeding [13] and is a method viruses and bacteria can hijack to enter cells [12], but despite its medical relevance it has been poorly studied so far, owing to its complex 3D dynamics making analysis difficult.

2. METHOD

2.1. Data acquisition and pre-processing

Dictyostelium cells expressing fluorescent markers for actin and PIP3 were recorded with a lattice light sheet microscope [14], yielding movies with planar pixel size 0.104 μm, z-spacing 0.162 μm, and frame rate 2–3 seconds. Whole cell segmentation was performed using the curvature-enhanced random walker [1]. Triangulated surface meshes were generated from these segmented images using Matlab's isosurface function, giving meshes with approximately 10^5 vertices. Fluorescence values were assigned to each vertex as outlined

Layer structure	Input	Output
Convolutional layer I/ PReLU/ dropout	$n \times 6$	$n \times 6$
Convolutional layer II/ PReLU/ dropout	$n \times 6$	$n \times 4$
Convolutional layer III/ PReLU/ dropout	$n \times 4$	$n \times 2$
Convolutional layer IV/ sigmoid	$n \times 2$	$n \times 1$ probability map

Table 1. Architecture of the GCN (n: number of nodes)

in [15]. Briefly, each vertex was assigned the maximum fluorescence value in each channel along a line scan normal to the surface. Line scans were truncated so that distance to the surface was always increasing along the line, preventing lines reaching other parts of the surface. Surfaces were manually annotated using MiCellAnnGELo [16], labelling the vertices of all cups in each frame and recording the locations of the centres of the cups. Binary vertex labels for the training set are 1 if a vertex is inside a macropinocytic cup, 0 otherwise, as shown in Figure 2**A**.

Graphs are defined by cell surface triangulations, with a 6-dimensional feature vector assigned to each vertex (x/y/z coordinates, two biomarker intensities, and Gaussian curvature). Coordinates and intensities were normalized to $[0, 1]$ within each time frame. The surface in each time frame was rotated randomly in 3 dimensions to prevent over fitting to coordinate data. Curvature is calculated using the trimesh python library (see [17] for details) without smoothing.

Two time-series containing 200 frames were processed as above, and split into training (180), and testing (20) datasets. From the training set 160 frames were used for training and 20 used for validation selected using 9-fold cross-validation. Test samples were manually selected such that they are significantly different from existing training data and have a high proportion of macropinocytic cups, in order to ensure a variety of unseen cups are used for testing.

2.2. Architecture and Optimization

The GCN uses convolutional layers [18] developed for node and graph classification, with the former being relevant here. It consists of 4 graph convolutional layers, using PReLU (with a parameter of 0.2) as a non-linear activation function, and dropout layers in between (see Table 1). The convolutional layers reduce the dimensionality of the feature vector until the last layer outputs a probability value, utilizing a sigmoid activation function. To optimize the weights, Adam optimization with a learning rate of 0.05 is used on a loss calculated from binary cross entropy. The model was trained for 250 epochs.

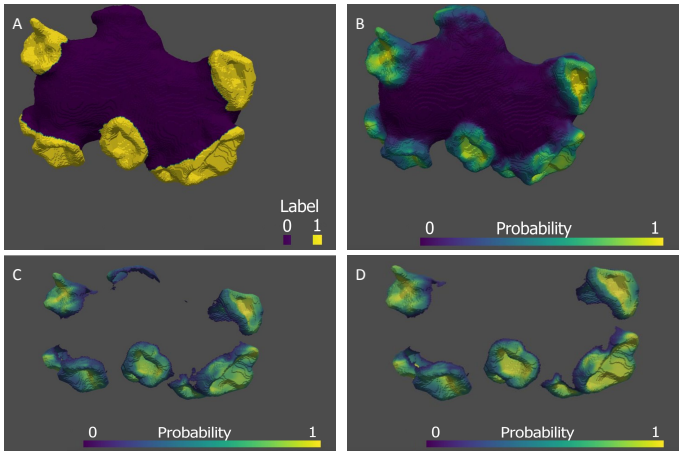

Fig. 2. **A**: Manually labelled input. Yellow: Macropinocytic cups; purple: Background. **B**: Probabilities to be part of a cup, predicted by the GCN model. **C**: Areas of the surface in **B** above the threshold. **D**: Segmented cups, given as the connected components of **C** above a minimum size.

2.3. Cup extraction

The model outputs a probability for each vertex of the mesh to be part of a macropinocytic cup, as shown in Figure 2**B**. For predicting cups on the surface, a threshold of 25% was applied to the probability map. Figure 3 shows averaged line profiles from the centre of a cup going outwards. As is expected, a probability of 50% is found at a distance where the annotated label drops off from 1. Biologically, a cup is however better defined by the extension of its PIP3 domain. PIP3 is a phospholipid signalling molecule in the cell membrane that regulates cup formation. The 25% probability threshold approximately coincides with where PIP3 drops to the background level outside a cup. It also defines where we find a good overlap between the ground truth cups and the predicted cups. However, manual annotation of ground truth cups is subjective and was done rather liberally, so that for the training set a small region outside of the cup boundary, which is mostly discernible by its high curvature, was still included in the annotation, as seen in Figure 2**A**. It is possible that the prediction provided by the model is closer to a useful definition at a 50% threshold where the probability intersects with the cup boundary defined by the highly curved rim.

Surfaces were then divided into connected components with label 1 in the predicted labelling. Components containing fewer than 1% of the total number of vertices were discarded. The remaining components represent separated predicted cups. An example of this method is shown in Figure 2. The same process was applied to the manual labels for assessing of individual cup detection accuracy in Section 3.1. Note that multiple cups that are touching each other on the surface are considered part of the same cup.

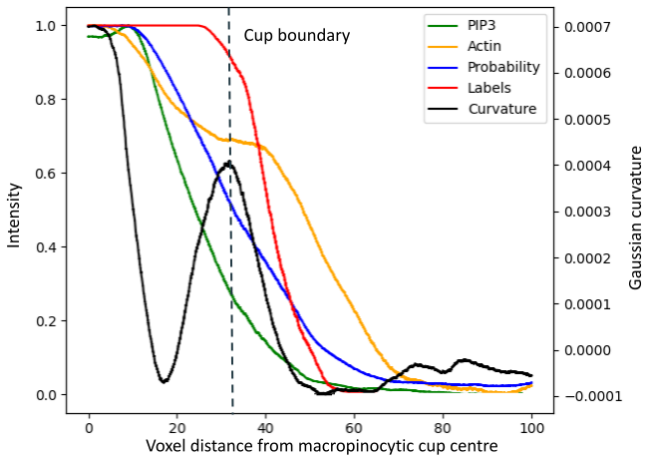

Fig. 3. Plot of the spatial distribution of features within cups, against the model prediction (probability to be inside a cup). Distances (geodesic) are given in units of image voxels. Fluorescence, curvature and annotated labels for each vertex are plotted against their distance from the nearest cup centre. Smoothing is applied as a moving average across each feature. Cup boundary delineates the area within a cup, extending up to the rim.

3. RESULTS AND DISCUSSION

3.1. Segmentation and detection

Results of the graph neural network are evaluated using the cell segmentation benchmark [19] and the Hausdorff distance, both adapted for application to surface feature detection. The cell segmentation benchmark is a combination of a segmentation score (SEG) and detection score (DET) used for comparing the accuracy of cell segmentation in images containing one or more cells. We apply this measure by considering segmentation of each cup as analogous to that of a cell in a multi-cell image, with mesh vertices replacing image pixels in this adaptation. The Hausdorff distance is a measure of how far apart two sets are at most. We apply this to our problem by again looking at each cup on the surface, using geodesic distance to measure the difference between prediction and ground truth.

The segmentation score (SEG) is based on the Jaccard index $J(S_{GT}, S_P) = |S_{GT} \cap S_P|/|S_{GT} \cup S_P|$, for a predicted cup vertex set S_P and the ground truth cup vertex set S_{GT}. The SEG score also requires that the matching criterion

$$|S_{GT} \cap S_P| > 0.5 \cdot |S_{GT}|$$

is met. The SEG score for a cup with ground truth vertices S_{GT} is 0 if no predicted cup satisfies the matching criterion, otherwise it is given as $J(S_{GT}, S_P)$ for matching a predicted cup with vertices S_P. The final SEG score for a frame is taken as the average over all ground truth cups. DET

Metric	Mean	Standard dev	Min	Max
SEG	0.79	0.04	0.71	0.86
DET	0.98	0.02	0.95	1.00
H	0.18	0.05	0.10	0.26

Table 2. SEG: Jaccard index of predicted cup regions and ground truth cups. DET: accuracy of detecting cups. H: Hausdorff distance

is calculated using:

$$\text{DET} = 1 - \frac{\min(\text{AOGMD}, \text{AOGMD}_0)}{\text{AOGMD}_0}$$

where AOGMD stands for Acyclic Oriented Graphs Matching Detection, measuring the model's ability to detect all important features in a single time frame, given by

$$\text{AOGMD} = \text{NS} + \text{FN} + \text{FP},$$

where NS (node split) is the number of predicted cups matched with more than one ground truth cup, FN (false negative) is the number of unmatched ground truth cups, and FP (false positive) is the number of unmatched predicted cups. AOGMD_0 represents a score for a graph with no predicted cups on the surface.

The Hausdorff distance is computed by comparing the boundary vertices of the sets S_{GT} and S_P for all pairs of sets meeting the matching criterion above. The distance from some point $p \in S$ to another set S' on a surface M is given as

$$d(p, S') = \min_{q \in S'} d_M(p, q),$$

where d_M is the geodesic distance on M. The Hausdorff distance H between S_{GT} and S_P is given by

$$H(S_{GT}, S_P) = \max\{\max_{p \in S_{GT}} d(p, S_P), \max_{q \in S_P} d(S_{GT}, q)\}.$$

To contextualise the result, the Hausdorff distance is calculated as a proportion of the diameter D of a predicted cup with vertex set S, given by

$$D = \max_{p,q \in S}\{d(p, q)\}.$$

The Hausdorff distance for each time frame is the mean value of H/D for all matched pairs S_{GT} and S_P.

Results are shown in Table 2, calculated across 20 unseen examples from a single time series. High DET values recorded suggest that the trained model is able to correctly identify macropinocytic cups with few errors and the SEG score indicates these identified regions have significant overlap with the ground truth. The Hausdorff distance is relatively high in these measurements, implying the cup boundary is harder for the model to correctly identify.

For comparison, Ostu threholding [20] was applied to the PIP3 channel of the test data, achieving mean scores of 0.44,

0.80, 0.35 across the SEG, DET and Hausdorff distance respectively. A better result was obtained through manually tuning a threshold value to the test dataset, (SEG $= 0.75$, DET $= 0.94$, Hausdorff $= 0.22$), but as shown in Figure 4, more complex cups cannot be fully characterised by PIP3 levels. Furthermore, applying this threshold to other frames produced much worse results (in some cases SEG$= 0.33$, DET$= 0.66$). Comparison to more recent approaches (e.g. [4, 7]) was not practical in the current study due to the different data formats required for these methods.

3.2. Macropinocytic cup analysis

By identifying macropinocytic cups on the cell surface it is possible to analyse the distribution of different fluorescent biomarkers associated with cups. An example can be found in Figure 3 where, for each vertex, the geodesic distance from the nearest manually identified centre of a macropinocytic cup is recorded. Using this distance to sort the vertices, the features PIP3, actin, and Gaussian curvature, along with manual labels are compared with the predicted label probability across the 20 unseen test examples. For clarification, each feature is smoothed after sorting, calculated using a moving average with a window of 5000 vertices, out of a total of approximately 10^5 vertices per frame.

Qualitative inspection helps determining the latent factors learnt by the model, and to confirm it is detecting relationships in the data that a simpler method such as colour thresholding could not achieve. Figure 4 shows two examples of paths through macropinocytic cups and their corresponding fluorescence, label, and predicted label probability values. The first one shows the model has learnt that areas of high intensity fluorescence are strong indicators of belonging to a macropinocytic cup, with the probability following closely the PIP3 profile. However, the more complex second example shows, that PIP3 alone is not necessarily a good proxy for defining cups. The prediction clearly employs a non-linear combination of features, demonstrating that GCNs are an ideal tool to tackle the problem of segmenting macropinocytic cups.

4. CONCLUSION AND FUTURE WORK

This paper demonstrates the utility of graph neural networks to answer biological questions on cell surface dynamics. Despite a relatively simple architecture, the GCN applied to our problem is able to successfully detect macropinocytic cups on the cell surface, which using filters operating on the 3D volume data would be very difficult to achieve. The network is able to segment these structures with reasonable accuracy, although this problem is ill-defined due to the irregularity of the cups making it difficult to produce ground truth annotations.

The two main results of this work are that 1) we are able to count cups, with applications in, for example mutant classification, and 2) by extracting macropinocytic cups we can track how distributions of signalling molecules and their effectors change over time, and analyse geometric features such as cup area, size, and perimeter, as well as their life span. All these measurements provide valuable insight into detailed mechanisms of cup formation.

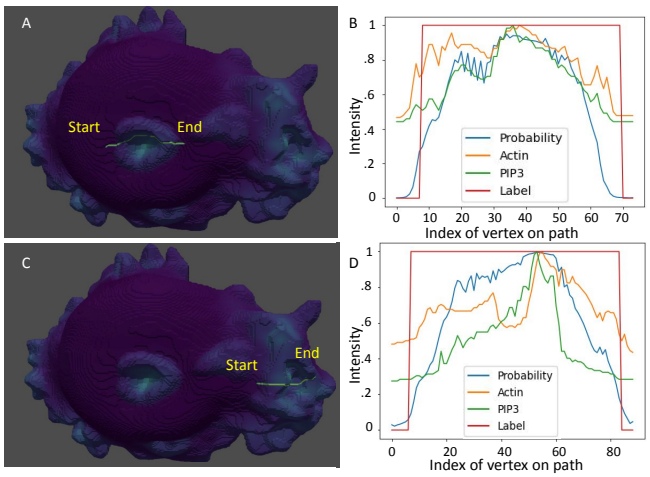

Fig. 4. Measuring surface values of individual cups. Lines drawn along the surface through two cups (**A,C**) with fluorescence, prediction, and input label values recorded along each line (**B,D**). While cup **A** shows prediction values closely aligned with PIP3 fluorescence (**B**), this pattern is not followed in the more complex cup **C**, as shown in **D**.

Building on this pilot study, we aim to utilise more complex network architectures in the future to improve segmentation accuracy and extend the model to apply to other fluorescent markers. Gao and Ji, for example, show how popular U-nets can be translated into the framework of GCNs [21]. Due to the generalized nature of neural networks, this approach is also applicable to other important biological problems, such as cell migration.

5. COMPLIANCE WITH ETHICAL STANDARDS

There are no conflict of interest. Cells used for experimentation are neither human or animal cells.

6. ACKNOWLEDGMENTS

This project is funded by the Engineering and Physical Science Research Council grant EP/V062522/1. The Warwick Lattice Light Sheet microscope was funded by The Wellcome Trust (208384/Z/17/Z).

7. REFERENCES

[1] E. Josiah Lutton, Sharon Collier, and Till Bretschneider, "A curvature-enhanced random walker segmenta-

tion method for detailed capture of 3D cell surface membranes," *IEEE Transactions on Medical Imaging*, vol. 40, no. 2, pp. 514–526, 2021.

[2] Assaf Arbelle, Shaked Cohen, and Tammy Riklin Raviv, "Dual-task ConvLSTM-UNet for instance segmentation of weakly annotated microscopy videos," *IEEE Transactions on Medical Imaging*, 2022.

[3] Dennis Eschweiler, Richard S Smith, and Johannes Stegmaier, "Robust 3D cell segmentation: Extending the view of cellpose," in *2022 IEEE International Conference on Image Processing (ICIP)*. IEEE, 2022, pp. 191–195.

[4] James G Lefevre, Yvette WH Koh, Adam A Wall, Nicholas D Condon, Jennifer L Stow, and Nicholas A Hamilton, "Llama: a robust and scalable machine learning pipeline for analysis of large scale 4D microscopy data: analysis of cell ruffles and filopodia," *BMC Bioinformatics*, vol. 22, no. 1, pp. 1–26, 2021.

[5] Carlos Castilla, Martin Maška, Dmitry V Sorokin, Erik Meijering, and Carlos Ortiz-de Solórzano, "3-D quantification of filopodia in motile cancer cells," *IEEE Transactions on Medical Imaging*, vol. 38, no. 3, pp. 862–872, 2018.

[6] Miguel Molina-Moreno, Iván González-Díaz, Jon Sicilia, Georgiana Crainiciuc, Miguel Palomino-Segura, Andrés Hidalgo, and Fernando Díaz-de María, "ACME: Automatic feature extraction for cell migration examination through intravital microscopy imaging," *Medical Image Analysis*, vol. 77, pp. 102358, 2022.

[7] Meghan K Driscoll, Erik S Welf, Andrew R Jamieson, Kevin M Dean, Tadamoto Isogai, Reto Fiolka, and Gaudenz Danuser, "Robust and automated detection of subcellular morphological motifs in 3D microscopy images," *Nature Methods*, vol. 16, no. 10, pp. 1037–1044, 2019.

[8] Jie Zhou, Ganqu Cui, Shengding Hu, Zhengyan Zhang, Cheng Yang, Zhiyuan Liu, Lifeng Wang, Changcheng Li, and Maosong Sun, "Graph neural networks: A review of methods and applications," *AI Open*, vol. 1, pp. 57–81, 2020.

[9] Karthik Gopinath, Christian Desrosiers, and Herve Lombaert, "Graph convolutions on spectral embeddings for cortical surface parcellation," *Medical image analysis*, vol. 54, pp. 297–305, 2019.

[10] Lebo Wang, Kaiming Li, and Xiaoping P Hu, "Graph convolutional network for fmri analysis based on connectivity neighborhood," *Network Neuroscience*, vol. 5, no. 1, pp. 83–95, 2021.

[11] Xiao-Meng Zhang, Li Liang, Lin Liu, and Ming-Jing Tang, "Graph neural networks and their current applications in bioinformatics," *Frontiers in genetics*, vol. 12, 2021.

[12] Jet Phey Lim and Paul A Gleeson, "Macropinocytosis: an endocytic pathway for internalising large gulps," *Immunology and Cell Biology*, vol. 89, no. 8, pp. 836–843, 2011.

[13] Cosimo Commisso, Shawn M Davidson, Rengin G Soydaner-Azeloglu, Seth J Parker, Jurre J Kamphorst, Sean Hackett, Elda Grabocka, Michel Nofal, Jeffrey A Drebin, Craig B Thompson, et al., "Macropinocytosis of protein is an amino acid supply route in Ras-transformed cells," *Nature*, vol. 497, no. 7451, pp. 633–637, 2013.

[14] Bi-Chang Chen, Wesley R Legant, Kai Wang, Lin Shao, Daniel E Milkie, Michael W Davidson, Chris Janetopoulos, Xufeng S Wu, John A Hammer III, Zhe Liu, et al., "Lattice light-sheet microscopy: imaging molecules to embryos at high spatiotemporal resolution," *Science*, vol. 346, no. 6208, pp. 1257998, 2014.

[15] E Josiah Lutton, Helena L E Coker, Peggy Paschke, Christopher J Munn, Jason S King, Rob R Kay, and Till Bretschneider, "The formation and closure of macropinocytic cups in a model system," *bioRxiv*, 2022.

[16] Adam Platt, E Josiah Lutton, and Till Bretschneider, "MiCellAnnGELo: Annotate microscopy time series of complex cell surfaces with 3D virtual reality," *arXiv preprint arXiv:2209.11672*, 2022.

[17] David Cohen-Steiner and Jean-Marie Morvan, "Restricted delaunay triangulations and normal cycle," in *Proceedings of the nineteenth annual symposium on Computational geometry*, 2003, pp. 312–321.

[18] Thomas N Kipf and Max Welling, "Semi-supervised classification with graph convolutional networks," *arXiv preprint arXiv:1609.02907*, 2016.

[19] Pavel Matula, Martin Maška, Dmitry V. Sorokin, Petr Matula, Carlos Ortiz-de Solórzano, and Michal Kozubek, "Cell tracking accuracy measurement based on comparison of acyclic oriented graphs," *PLoS one*, vol. 10, no. 12, pp. 1–19, 12 2015.

[20] Nobuyuki Otsu, "A threshold selection method from gray-level histograms," *IEEE transactions on systems, man, and cybernetics*, vol. 9, no. 1, pp. 62–66, 1979.

[21] Hongyang Gao and Shuiwang Ji, "Graph u-nets," in *international conference on machine learning*. PMLR, 2019, pp. 2083–2092.